Staurosporine-Induced Apoptosis in Human Cornea Epithelial Cells In Vitro

Steffen Härtel,[1–4]* Michaela Zorn-Kruppa,[1] Svitlana Tykhonova,[1] Päivi Alajuuma,[5] Maria Engelke,[1] and Horst A. Diehl[1]

[1]University of Bremen, Institute of Biophysics, Bremen, Germany
[2]Facultad de Ciencias Químicas, Departamento de Química Biológica, Pabellón Argentina, Universidad Nacional de Córdoba, Ciudad Universitaria, Córdoba, Argentina.
[3]Centro de Estudios Científicos, Arturo Prat 514, Valdivia, Chile
[4]Instituto de Física, Universidad Austral de Chile, Valdivia, Chile
[5]Santen Oy, Tampere, Finnland

Received 21 February 2003; Revision Received 12 May 2003; Accepted 29 May 2003

Background: Apoptosis is a an important process in corneal development, homeostasis, and disease. This study was performed to determine for the first time basic temporal apoptotic features of SV-40 immortalized human corneal epithelial (HCE) cells. Additionally, we introduce a sensitive analysis of confocal microscopic images to measure the kinetics of staurosporine (STS) induced phosphatidylserine (PS) membrane translocation and early nuclear morphological changes.

Methods: HCE cells were cultured in the presence of STS to induce apoptosis. Caspase-3 activity was measured with the fluorogenic substrate z-DEVD-rhodamine 110. We determined mitochondrial viability with a 4-[3-(4-iodophenyl)-2-(4-nitrophenyl)-2H-5-tetrazolio]-1,3-benzenedisulfonate reduction assay, and chromatin degradation with a fluorometric method using 4,6-diamidino-2-phenylindole (DAPI). Membrane translocation of PS and nuclear alterations were assessed by quantitative fluorescence microscopy. Image processing routines were written in interactive data language (IDL).

Results: Nuclear alterations like hyperchromicity, pyknosis, and active chromatin reorganization evolved instantly after STS induction. They were followed by PS translocation, DNA fragmentation, mitochondrial breakdown, and caspase-3 activation, which were detected between ≈90 min and 4 h.

Conclusions: Morphological and texture sensitive descriptors proved to be highly susceptible for the quantification of early apoptotic nuclear characteristics in HCE cells. We propose this method to be considered for the detection of subtle nuclear reorganization in cellular studies. Cytometry Part A 55A:15–23, 2003.

Key terms: apoptosis; human cornea epithelium; image processed quantitative fluorescence microscopy; chromatin texture; chromatin condensation; hyperchromicity; staurosporine

Apoptosis is a genetically determined process, which is guided by a succession of distinct morphological and biochemical events. Apoptosis can be induced by a variety of physical, chemical, and biological stimuli, including exposure to cytotoxic agents (1). As an important difference to necrosis, apoptotic cell death does not provoke inflammatory reactions in the tissue and is therefore a key mechanism for the removal of cells during embryogenesis and tissue homeostasis throughout the lifetime of higher organisms. Malfunction of the regulatory molecular machinery of apoptosis during its initiation, its progression, or the execution phase is involved in the pathophysiology of several important diseases (2,3).

In the eye, cornea epithelium cells present a direct target for different kinds of mechanical injury, infections, ultraviolet exposure, or photorefractive keratectomy (4–7). It has been recognized that the corneal epithelium has a rapid self-renewing capacity. Epithelium cells are of elevated interest because they not only sense and process information about stress internally, but also mediate signals into deeper layers of the cornea through secretion of Fas ligands. Fas directly induces apoptosis in keratocytes, which minimizes integral tissue damage and preserves the

Contract grant sponsor: European Union; Contract grant number: BMH4-97-2324; Contract grant sponsor: Alexander v. Humboldt Foundation (Germany); Contract grant sponsor: CONICET (Argentina); Contract grant sponsor: FONDECYT (Chile); Contract grant number: 3030065.

Steffen Härtel and Michaela Zorn-Kruppa contributed equally to this manuscript.

*Correspondence to: Dr. Steffen Härtel, Centro de Estudios Científicos (CECS), Arturo Prat 514, Casilla 1469, Valdivia, Chile.
E-mail: shaertel@physik.uni-bremen.de

Published online in Wiley InterScience (www.interscience.wiley.com).
DOI: 10.1002/cyto.a.10068

transparency of the cornea (8). Fas ligand secretion is supposed to be a prerequisite for the success of human cornea transplants, where a very high percentage is accepted without immunosuppressive therapy (9). Although apoptosis has been detected in various diseases of injured cornea, there is a lack of detailed information about specific apoptotic features in cornea epithelium cells.

In the present study, we focus on the time resolved quantification of apoptotic parameters in an immortalized human cornea epithelium (HCE) cell line. The SV-40–transformed HCE cell line is well characterized and has been used as an in vitro model for ocular irritation (10). For the induction of apoptosis we use staurosporine (STS), which is a nonspecific serine-threonine kinase inhibitor, working effectively in several cell types including corneal epithelium (11). We quantify: (i) the mitochondrial viability, (ii) the proteolytic activity of caspase-3, (iii) the translocation of phosphatidylserine (PS) from the inner to the outer membrane layer, (iv) the chromatin degradation in high and low molecular weight DNA, and (v) alterations in the chromatin structures of the cellular nuclei. Characteristics i, ii, and iv were assessed by frequently used commercial assays for suspended cell populations. For the quantification of PS translocation and early chromatin condensation in adherent HCE cells instead, we introduce a sensitive approach based on image processed quantitative fluorescence microscopy (QFM). Our results describe for the first time the occurrence and the temporal succession of apoptotic key-characteristics in SV-40 immortalized HCE cells. The time resolved quantification of distinct apoptotic features elucidates causal relationships between the involved molecular mechanisms, which are essential for a better interpretation of toxic events in the eye. Finally, the introduced technique based on texture sensitive image processed QFM should be taken into consideration for the refinement of toxicity test methods in adherently growing cell cultures in the future.

MATERIALS AND METHODS

HCE Cells

HCE cells were grown in culture medium containing Dulbecco's Minimum Eagle's Medium and Ham's nutrient mixture F-12 (Gibco BRL, Paisley, Scotland) 1:1 supplemented with 15% (v/v) fetal calf serum (Gibco BRL), 1% (v/v) antibiotic, antimycotic solution containing penicillin 10.000 U/ml, streptomycin 10.000 μg/ml and amphotericin B 25 μg/ml (Gibco BRL), 2 mM L-glutamine (Gibco BRL), 5 μg/ml insulin (Sigma-Aldrich, Steinheim, Germany), and 10 ng/ml human epithelial growth factor (Sigma-Aldrich, Steinheim, Germany). The cells were grown in filter-capped 25 cm^2 TC-flasks (Nunc, Wiebaden, Germany) and passaged at a split ratio of 1:4 three times a week. STS (4 mM in dimethyl sulfoxide; Alexis Deutschland, Grünberg, Germany) was diluted with cell medium before each experiment.

Caspase-3 Activity

Caspase-3 activity was determined with a caspase-3 kit (Molecular Probes Europe, Leiden, Netherlands), based on the fluorogenic substrate z-DEVD-rhodamine 110. Two to four hours after the addition of STS, 1–2 × 10^6 HCE cells were collected by trypsinization and centrifugation. Cells were washed with phosphate buffered saline, resuspended in 50 μl lysis buffer, and incubated on ice for 30 min. The lysate was centrifuged at 5000 rpm for 5 min to pellet the cellular debris. Fifty microliters of the supernatants were mixed with 50 μl substrate containing reaction buffer (20 mM piperazine-1,4-bis(2-ethanesulphonic acid) (PIPES), pH 7.4, 4 mM ethylene-diamine-tetraacetic acid [EDTA], 0.2% 3-[(3-cholamidopropyl) dimethylammonio]-1-propane-sulfonate (CHAPS), 10 mM dithiothreitol, and 50 μM z-DEVD-rhodamine 110 substrate), covered, and incubated for 30 min. Finally, fluorescence was measured with a LS50B fluorescence spectrometer (Perkin-Elmer, Überlingen, Germany) using 496/520 nm as excitation/emission wavelength.

Mitochondrial Activity and Cell Viability

Cell viability was measured with the 4-[3-(4-iodophenyl)-2-(4-nitrophenyl)-2H-5-tetrazolio]-1,3-benzene disulfonate (WST-1) reduction assay for mitochondrial activity (Roche Diagnostics, Mannheim, Germany) (12). HCE cells were seeded in 96-well tissue culture plates (Corning-Costar, Shihol-Rijk, Netherlands) in a density of 1.5/3 × 10^4 per well for long-/short-term incubation. After 24 h, medium was replaced and cells were incubated for indicated time periods in the presence or absence of STS. Thereafter, medium was replaced by a serum-free medium and incubated for 1 h. WST-1 reagent was added in a volume of 1:10 and incubated for 1 h. Samples were shaken for 1 min before measuring the absorbance with an automated MRX microtiter plate reader (Dynatech Medical Products Ltd., West Sussex, UK). Control values were set to 100% and the effective dose value (EC_{50}) was calculated from the dose response curve using GraphPad Prism program (GraphPad Software, Inc., San Diego, CA).

DNA Fragmentation

DNA fragmentation in HCE cells was examined according to a previously described procedure (13), with slight modifications. Cells were pelleted into tubes, washed once with phosphate buffer, and lysed in 600 μl 10 mM Tris buffer (pH 7.4) containing 3 mM EDTA and 0.2% Triton X-100 for 25 min on ice. Tubes were centrifuged at 27,000*g* for 20 min to separate the high and low molecular weight (MW) DNA fragments. Pellets containing non-fragmented, chromosomal DNA (high MW) were resuspended in 600 μl lysis buffer and sonicated for 1–2 min. The amount of DNA was determined by the fluorometric method using 4,6-diamidino-2-phenylindole (DAPI; Molecular Probes Europe). Ten to fifty microliters of a DNA sample was added to 3 ml of the reagent (100 ng/ml DAPI in 10 mM Tris, pH 7.4, containing 10 mM EDTA and 100 mM NaCl). Fluorescence intensities were measured at 355/455 nm excitation/emission wavelengths. Addition of DNA solution was repeated 4 times. The ratio of fragmented to chromosomal DNA (low/high MW) was calculated from the increase of the fluorescence intensity. Additionally, the apoptotic nature of the DNA fragmentation

was proved by enzyme-linked immunosorbent assay (ELISA) according to the manufactur's manual (Boehringer Mannheim, Mannheim, Germany). ELISA detects bromodeoxyuridine-labeled DNA fragments in cell lysates (apoptosis) and culture supernatants (necrosis or late apoptosis).

Microscopical Analysis of PS Translocation and Morphological Changes in HCE Nuclei

Fluorescence imaging was performed with laser scanning microscopes (LSMs; Zeiss 410 or 510, Göttingen, Germany), equipped with a 488 nm wavelength argon ion laser and a water-heated, gas-equilibrated microscopic incubator for long-time cell analysis.

Calculation of the mean area covered by individual HCE cells. HCE cells were transferred into 8-well culture chambers (Nunc, Wiesbaden, Germany) of the microscopic incubators. After 12 h, SYTO-13 (Molecular Probes Europe) live-cell nucleic acid stain (5 mM in dimethyl sulfoxide) was added to the cell chambers in a final concentration of 100 nM. Two-channel picture series were recorded by LSM (excitation: 488 nm; intensity $I[x,y] \in [0,255]$, $x/y \in [0,511]$ pixels): channel 1, brightfield pictures; channel 2, 505–530 nm band pass filter for SYTO-13 fluorescence. All image processing routines were written in interactive data language (IDL, Research Systems Inc., Boulder, CO.). Segmentation of HCE cells from channel 1 was based on the scaling-index method (14). Segmentation of HCE nuclei (channel 2) was achieved by fixing a threshold value I_T in the intensity histogram of the channels. Both procedures were completed by a successive treatment with opening/closing operators (15). Slight heterogeneities in the segmentation of HCE nuclei were corrected manually (PhotoStudio, ArcSoft Inc., www.arcsoft.com). The mean area covered by individual HCE cells was calculated by dividing the total area covered with cells by the total number of detected nuclei ($N \approx 100$).

Morphological changes in HCE nuclei. One hour after SYTO-13 staining, 0.5-2 μM of STS was added to cell samples and fluorescence image series were recorded every 3 min for 3 h. For the parameterization of STS induced changes in HCE nuclei, we calculated a series of morphological parameters and textural features from the fluorescence distribution of the SYTO-13–stained chromatin. For each segmented nuclei, we calculated the nuclear size **A** (number of pixels). The perimeter **P** was estimated from the number of border pixels, identified with a four-neighbor algorithm (15). From **P** and **A**, the simple, zoom invariant morphologic descriptor $\mathbf{P^2/A}$ was derived. The fluorescence density **I/A** was calculated from the ratio of the total fluorescence intensity of each nuclei and its respective size. The textural feature Simple Entropy (S') was derived by two steps: (i) summing the intensity differences $|\Delta I|$ in the vicinity ϵ of each pixel [x,y] of the nuclei: $S[x,y] = \sum (|\Delta I_\epsilon| + \ln[|\Delta I_\epsilon|])$; and (ii) calculating the sum i of all nuclear pixels: $S' = \sum S[x_i,y_i]$. Further texture sensitive features were adapted from Haralick et al. (16), who introduced more than 10 parameters for the characterization of a co-occurrence matrix **C**, calculated for an image or an image region. In our case, the fluorescence intensity distribution for each segmented nuclei was normalized into 15 intensity intervals $I'(x,y) \in [0,14]$ in order to obtain reasonably sized **C** ($\dim[15 \times 15]$). Intensity noise for each nuclei was eliminated slightly by a 3×3 median filter. For this study, the parameters Entropy and the 2nd Angular-Moment were calculated from **C**.

PS translocation. 0-6 h after the induction with 0.5-2 μM STS, a fluorescent cocktail containing annexin V plus fluorescein isothiocyanate (AV) and propidium iodide (PI) was added to the cell chambers to a final concentration of 1:10. The AV/PI cocktail was prepared by adding 20 μl of AV stock solution (Boehringer Mannheim) and 20 μl of PI stock solution (50 μg/ml, HEPES, 10 mM HEPES/NaOH, 140 mM NaCl, 5 mM $CaCl_2$, pH 7.4) to 1 ml HEPES buffer. After stabilization of the fluorescence signals at room temperature (≈30 min), 3-channel picture series (excitation: 488 nm; $I[x,y] \in [0,255]$, $x/y \in [0,511]$) were recorded: channel 1, brightfield picture; channel 2, 515–525 nm band pass filter for AV fluorescence; channel 3, 600 nm long pass filter for PI fluorescence (Fig. 2A–C). Segmentation of the total area covered by HCE cells ($AV^+ + AV^-$) was achieved as described above. Segmentation of PS-exposing membranes which bind AV (AV^+), and of HCE nuclei accessible to PI (PI^+) was achieved by fixing threshold values in the intensity histograms of the respective fluorescence channels and treatment with opening/closing operators. The percentage of outer membrane area without PS (AV^-) was calculated by $(AV^-)/(AV^+ + AV^-) \times 100$. The total number of cells in a picture series ($PI^+ + PI^-$) was calculated from the area covered with membranes ($AV^+ + AV^-$) divided by the mean area of one HCE cell (step 1). The number of unstained nuclei (PI^-) was calculated by $(PI^+ + PI^-) - (PI^+)$. Finally, we derived the number of: (i) cells showing secondary necrosis (PI^+/AV^+) from the co-occurrence of (PI^+) nuclei with (AV^+) membranes (square III, Fig. 4A–C), (ii) cells showing apoptosis (PI^-/AV^+) (square II, Fig. 2A–C) from the number of cells with (AV^+) membranes minus cells in secondary necrosis (PI^+/AV^+), (iii) cells showing necrosis (PI^+/AV^-) (square IV, Fig. 2A–C) from the co-occurrence of (PI^+) nuclei which (AV^-) membranes, and (iv) "healthy" cells (PI^-/AV^-) (square II, Fig. 2A–C) from the number of cells with (AV^-) membranes minus necrotic cells (PI^+/AV^-).

RESULTS

Mitochondrial Viability and Caspase-3 Activation

In order to find an appropriate concentration range for STS induced cell death, decrease in mitochondrial dehydrogenase activity was determined with a WST-1 response curve. We obtained an EC_{50} at 0.5 μM and EC_{99} at 1 μM, and used 0.5–2 μM STS for all further experiments. Changes in the viability of HCE cells were not found before 4 h with 2 μM STS (Fig. 1A). The cleavage of the fluorogenic substrate z-DEVD-rhodamine 110 to its fluorescent product by activated caspase-3 is shown in Fig. 1B. No significant increase of caspase-3 activity could be detected before 4 h after STS treatment.

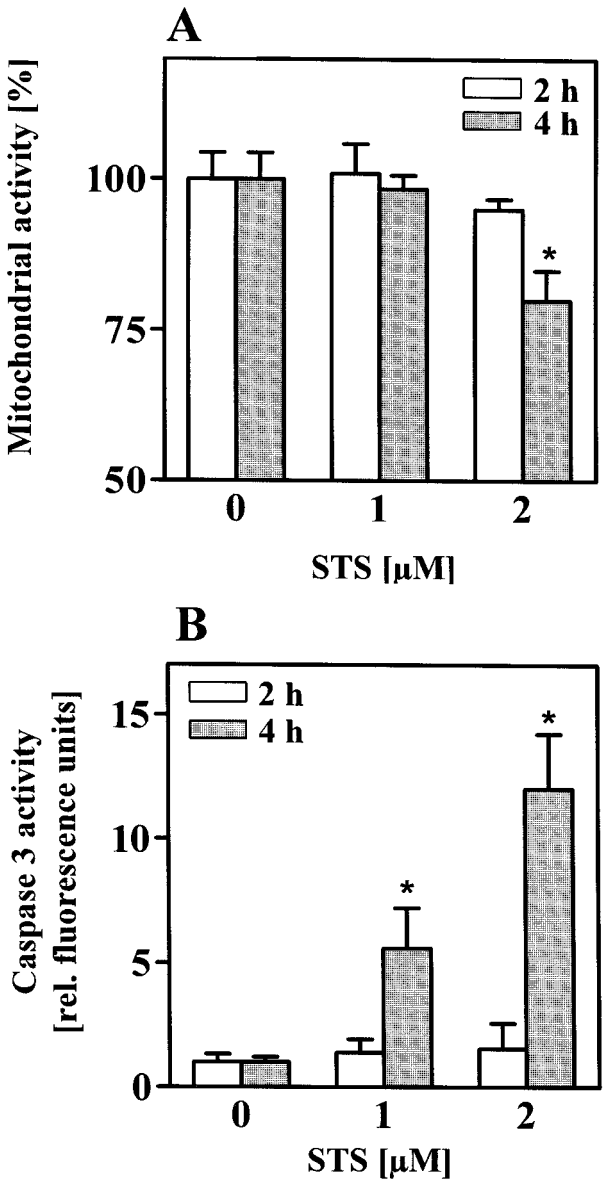

FIG. 1. Time course of apoptotic parameters in HCE cells as determined 2 and 4 h (white/hatched bars) after the induction with 1 and 2 μM STS. **A:** Mitochondrial activity with respect to control cells (100%), as determined with the WST-1 reduction assay. **B:** Activation of caspase-3 as determined by the relative fluorescence intensity of the fluorogenic substrate z-DEVD-rhodamine 110. Bars represent mean values of three independent experiments ± standard error of the mean. *Significant deviations from control values, $P < 0.05$.

PS Translocation

PS translocation can be visualized by fluorescence staining with the phospholipid-binding protein AV (17). Cellular counter-staining with AV and PI allows the classification of unstained/healthy (AV^-/PI^-), early apoptotic (AV^+/PI^-), necrotic (AV^-/PI^+), and secondary necrotic cells (AV^+/PI^+). We determined STS induced PS externalization by QFM directly inside the microscopic incubation chambers. Here, automated segmentation of membranes from bright field pictures presents a difficult task because HCE cells naturally lack contrasting pigments (Fig. 2A). Nevertheless, we achieved precise segmentation of cells with a nonlinear digital filter class based on the scaling-index method (14).

Figure 2D shows that untreated HCE cells hardly showed any AV/PI fluorescence; 95% of the cells are quantified as "healthy" (square I, Fig. 2A–C). Between 2 and 4 h, all major changes in the AV/PI fluorescence occurred. The number of apoptotic/secondary necrotic cells increased intensively (square II/III, Fig. 2A–C). For 1 μM STS, a sigmoid Bolzmann fit of the apoptotic cell population revealed a change of 20% at 1 h 47 min, of 50% at 2 h 28 min, and of 80% at 3 h 9 min (Fig. 2D, inset). For the secondary necrotic cell population, the respective changes occurred at 2 h 56 min, 3 h 15 min, and 3 h 35 min. The earliest significant increase of the apoptotic cells occurred after 90 min ($P < 0.05$). The described kinetics also reflects the effects of STS concentrations of 0.5 and 2 μM (data not shown).

DNA Fragmentation and Chromatin Condensation

Figure 3A shows that oligonucleosomal DNA fragmentation in HCE cells started to increase 2 h after STS treatment. DNA fragmentation increased in a time- and dose-dependent manner until the cytosolic fragments added up to a maximum of ≈60% after 24 h. Thereafter, incubation resulted in lower fragmentation ratios, indicating the occurrence of secondary necrosis which is characterized by membrane disintegration and cell lysis at a late stage of apoptosis (18). In consequence, cells release fragmented DNA into the extracellular medium, which is washed away prior to the externally induced cell lysis, and lost for further quantification. In addition to the DAPI method, bromodeoxyuridine-labeled DNA fragments were detected with ELISA 7 h after STS induction (data not shown).

In Figure 3B and C, the time course of the normalized mean values of 6 morphologic parameters and textural features from the fluorescence distribution of SYTO-13 stained HCE nuclei are plotted. SYTO-13 fluorescence precisely marks off chromatin substructures (Fig. 4), which is essential for the reliable application of image processing routines. As can be observed in Figures 3B and 4A,B, a pronounced increase of nuclear fluorescence staining (**I/A**) became notable during the first 10 min after STS was added to the incubation chambers (0.5–2 μM). **I/A** reached a plateau after ≈20 min. Parallel to the hyperchromicity, the nucleoli structures started to fray and condensed peripherally towards the nuclear membrane unto an almost complete structural disintegration (Fig. 4D,F). This observation was parameterized sensitively by different textural descriptors: the 2nd Angular Moment, Haralicks Entropy, and S′ (Fig. 3C). The time course of S′ is quite similar to **I/A**, reaching a plateau after 10–20 min. The 2nd Angular Moment also quantifies these fast initial changes of the textural properties, but reached its saturation level not before ≈2 h. Haralicks Entropy instead showed to be insensitive to early changes. Like the 2nd Angular Moment, this parameter decayed gradually for ≈2 h.

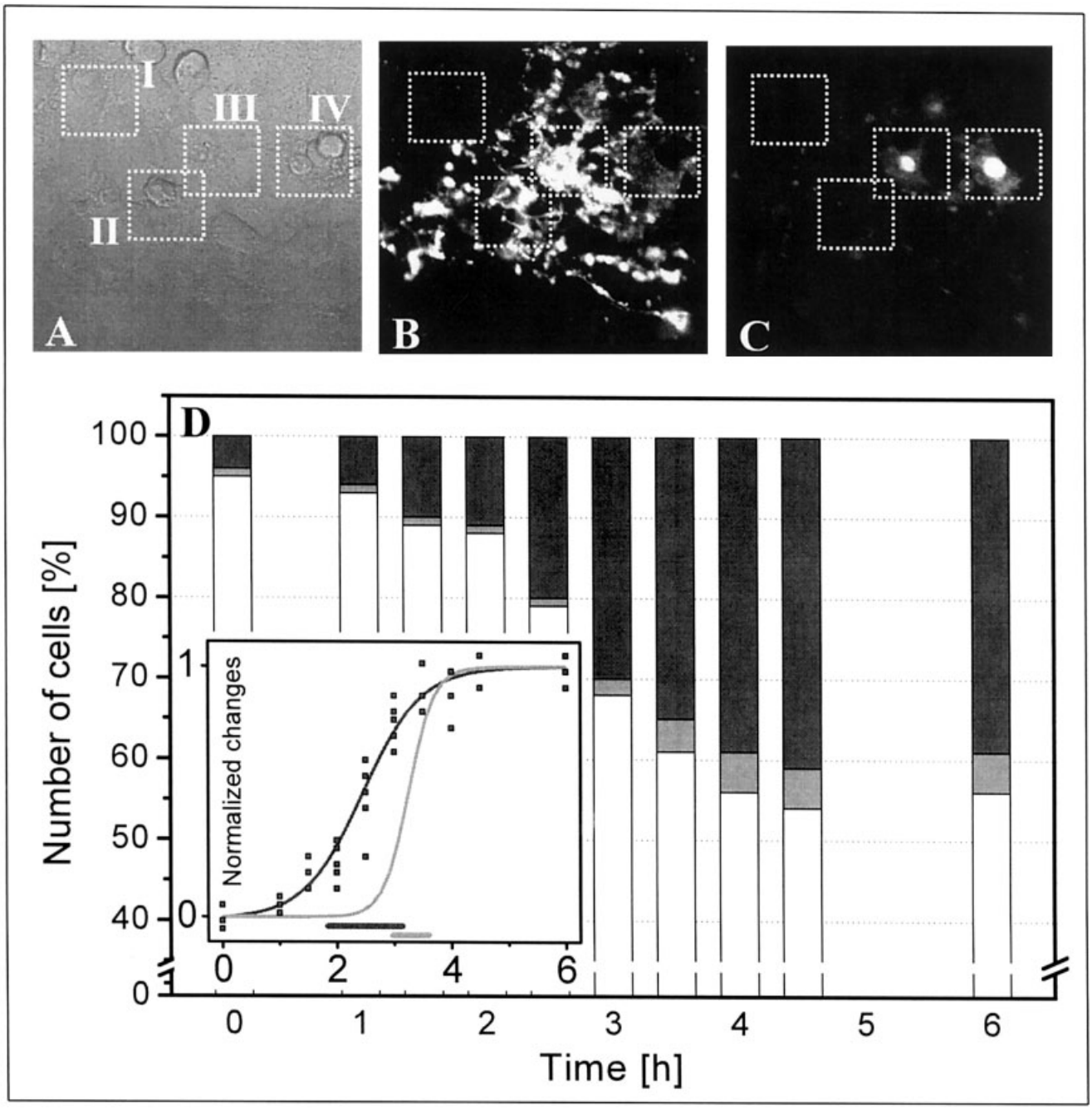

FIG. 2. Time course of apoptosis in adherent HCE cells, as analyzed by QFM (λ_{exc} = 488 nm) in combination with the fluorophores AV and PI. AV binds to PS, exposed on the outer membrane surface. PI stains cellular nuclei of HCE cells which have lost its membrane integrity. Squares (I–IV) in digital microscopic image channels (A–C) show all possible combinations of fluorescence staining in cultured HCE cells. **A:** Brightfield channel. **B:** AV fluorescence channel (λ_{em} = 515–525 nm). **C:** PI fluorescence channel (λ_{em} > 600 nm). **D:** Time course of apoptosis in HCE cells after induction with 1 μM of STS. White bars mark the percentage of normal, vital cells (AV^-/PI^-) (compare to square I in A–C). Gray bars mark the percentage of apoptotic cells (AV^+/PI^-) (square II), and light gray bars mark the percentage of necrotic/late apoptotic cells (AV^+/PI^+) (square III). Necrotic HCE cells, as identified in square IV, were not detected in a significant number. Bars indicate means of 3–6 independent experiments. Inset shows the time resolved experimental data for 1 μM STS of the relative apoptotic (gray squares and curve) and secondary necrotic (light gray) HCE cell population in combination with the respective sigmoid Bolzmann fit. For the apoptotic cell population, 20%, 50%, and 80% of the changes occurred at 1 h 47 min, 2 h 28 min, and 3 h 9 min (the time interval is marked by a gray line). For the secondary necrotic cell population, the respective changes occurred at 2 h 56 min, 3 h 15 min, and 3 h 35 min (light gray line). The earliest detection of a significant PS translocation was detected after 90 min ($P < 0.05$).

The size of the segmented HCE nuclei does not change during the first ≈20 min of STS induction (Fig. 3B). After 20 min, the nuclei shrink for about 40 min, loosing ≈10% of their original area. Prior to the shrinkage of the nuclei, the shape begins to be altered after ≈10 min. The transition from the dominant circular aspect of the nuclei with

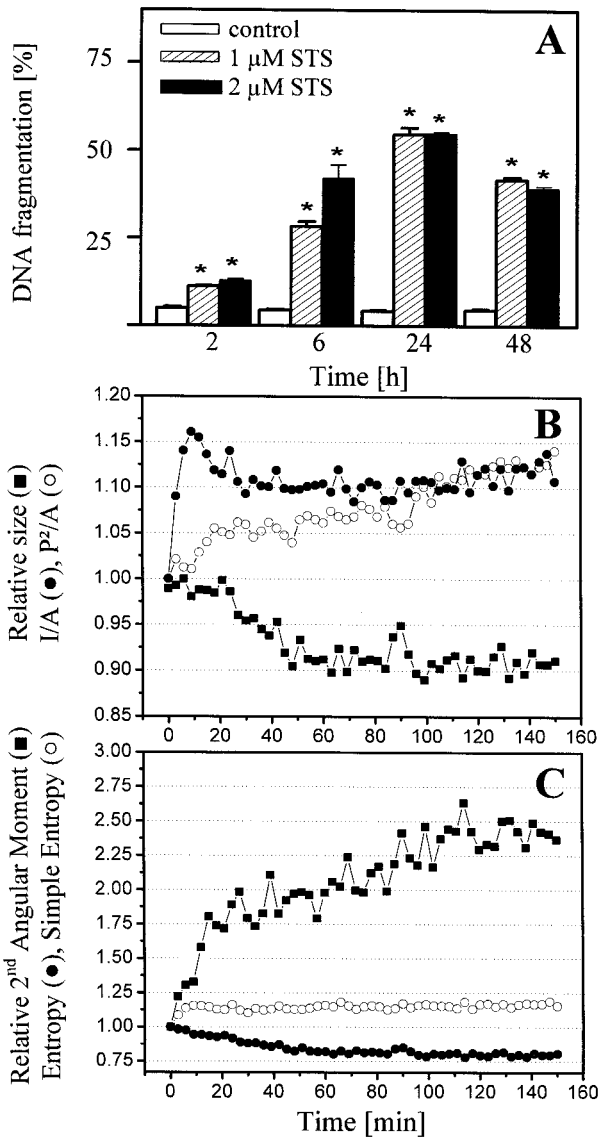

FIG. 3. The effects of STS on biochemical, morphological, and texture parameters of HCE nuclei. **A:** DAPI fluorescence determines DNA fragmentation (100 × cytosolic DNA content/total DNA) of nonconfluent HCE cells 2–48 h after exposure to STS. The cytosolic DNA content (low MW) and total DNA (low MW + high MW) were determined as described in Materials and Methods. DNA fragmentation in control cells (white bars) is compared to DNA fragmentation in cells treated with 1 or 2 μM STS (striped/black bars). Bars indicate mean values ± standard error of the mean from 3 independent experiments. *Significant differences from control values, $P < 0.05$. **B:** STS induced changes of the nuclear size **A** (solid squares), the fluorescence density of SYTO-13 stained nuclei **I/A** (solid circles), and the zoom invariant morphologic parameter $\mathbf{P^2/A}$ (open circles). **C:** STS induced changes on the texture of nuclear chromatin structures: Haralicks 2nd Angular Moment (solid squares), Haralicks Entropy (solid circles), and S′ (open circles). For B and C, parameters were derived from image sequences ($\Delta t = 3$ min) as defined in Materials and Methods. Mean values of ≈40 segmented cell nuclei are plotted for each respective parameter. The mean values of the control nuclei ($t \leq 0$, compare to Fig. 4A,E) were normalized to 1.

isolated nucleoli to more elongated shapes with peripherally condensed chromatin can be observed in Figure 4A–F. While the vast majority of the HCE nuclei follow the described patterns, only very few nuclei (≈1%) provided characteristics of a karyorrhexis, which is accompanied by condensed nuclei and clumped chromatin (Fig. 4G).

DISCUSSION

The overall time course and the concentration range of STS induced apoptosis in SV-40 immortalized HCE cells is in good agreement with apoptotic key-characteristics, detected in primary corneal epithelial cells (19), in cerebrocortical cultures (20), or in cultured lymphoma cells (21). In the present model of the apoptotic pathway, the liberation and activation of caspase-3 from the intermembrane space of the mitochondria has been described as an early apoptotic event, leading to successive cleavage of a number of different proteins, including poly(ADP-ribose) polymerase and DNA-dependent protein kinases (22,23). The activation of Ca/Mg-dependent nucleases, which degrade chromosomal DNA into high or low MW fragments, is generally accepted as a comparatively late event in the apoptotic schedule (24). In HCE cells, possible temporal differences between the reduction of mitochondrial activity and caspase-3 activation cannot be resolved within the applied methodology (Fig. 1). Rather surprisingly, oligonucleosomal DNA fragmentation was detected as early as 2 h post induction (Fig. 3A), which questions the necessity of mitochondrial disruption or caspase-3 activation for the initiation of DNA cleavage in HCE cells.

Another key-feature, frequently categorized as an early apoptotic event is the membrane translocation of PS. Most apoptotic cell types externalize PS, which presents an activating signal for ambient macrophages (17,25). In HCE cells, PS translocation was initiated not before 90 min after STS induction (Fig. 2D). Between the initiation of the PS translocation and the beginning of the saturation level, the major part of the reorganization occurs within 1 h 30 min (Fig. 2D, inset). This time scale cannot be explained by passive diffusion; it suggests the involvement of active proteins, which regulate the lipid asymmetry between the plasma membrane layers (26). Surprisingly, the final percentage of membrane surface which exposes PS does not exceed ≈45% of the total cell population, independent of the applied STS concentration of 0.5–2 μM. Individual HCE cells either did or did not expose PS, whereas partial PS translocation did not occur (Fig. 2B). In contrast, the entire cell population expressed severe peripheral chromatin condensation (Figs. 3, 4). Therefore, STS induced apoptotic chromatin condensation is not necessarily followed by PS translocation in HCE cells.

For the detection of early chromatin changes, SYTO dyes have already been used successfully (27). We observed hyperchromicity of DNA (increased **I/A**) and reorganization of the chromatin structure in HCE nuclei (all texture sensitive parameters) almost instantly after STS induction (Figs. 3, 4). This surprisingly fast reorganization preceded all other apoptotic features and showed morphologic characteristics of a "peripheric chromatin condensation" (23). Hyperchromicity and peripheric chromatin reorganization were also accompanied by nuclear pyknosis (A) and deformation of the circular nuclei of healthy cells ($\mathbf{P^2/A}$) (Figs. 3B,C, 4E,F). It should be empathized that the presented size-, shape-, and texture-sensi-

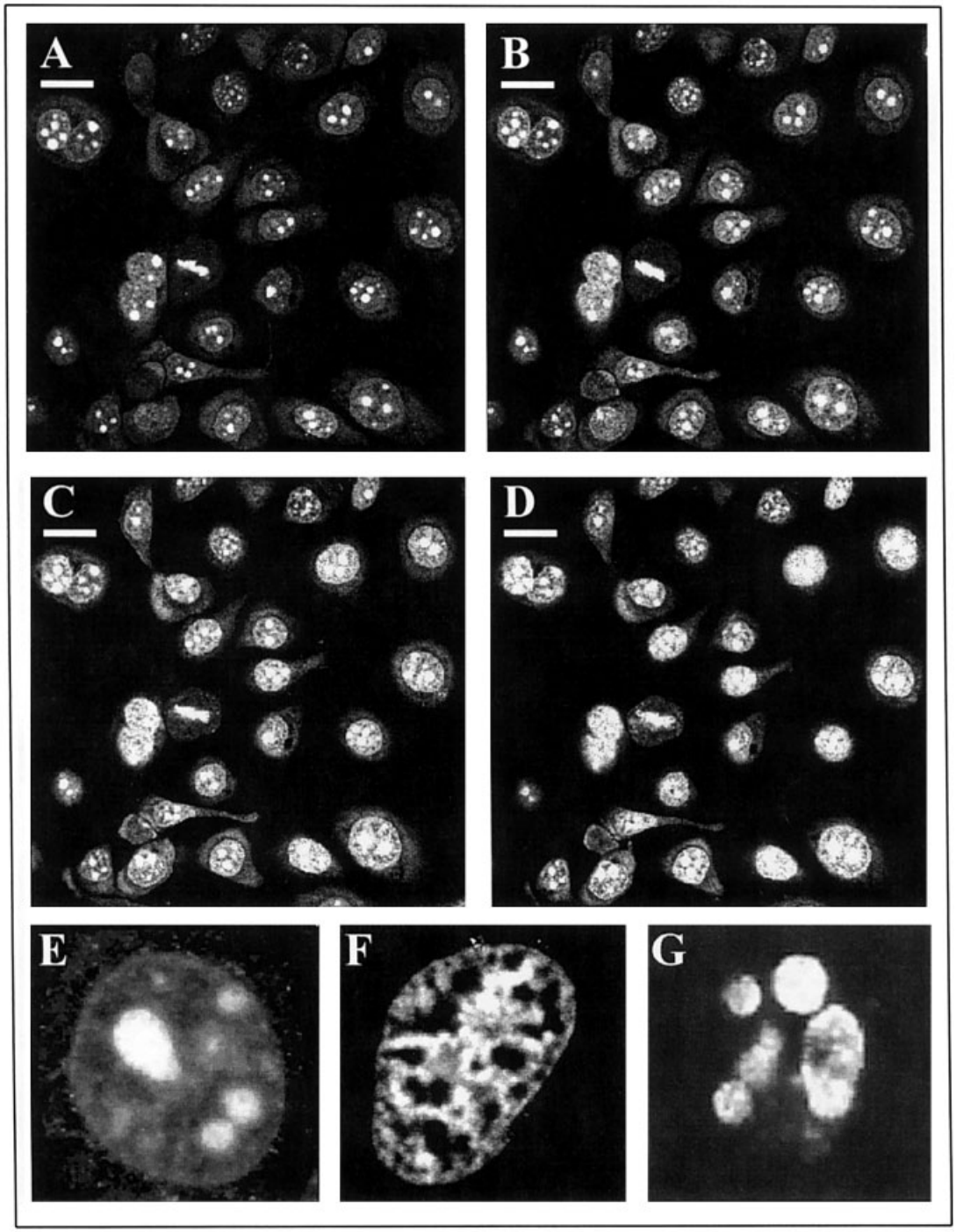

FIG. 4. Visual effects of STS on nuclear morphology of HCE cells. Confocal images (A–D) show SYTO-13 fluorescence after induction with STS (2 μM). **A:** 0 min (control). **B:** 10 min. **C:** 30 min. **D:** 60 min (cf. Fig. 3B,C). HCE nuclei show time-dependent increase of integral fluorescence density (hyperchromicity). B: Nucleoli substructures start to disappear as soon as 10 min after STS treatment. A–D: Bars in the upper left corners mark 20 μm. E–G: Confocal images show representative details of chromatin organization in HCE nuclei. **E:** "Normal" chromatin structure. **F:** Peripheric chromatin condensation, 2 h after STS induction (2 μM), shown by a vast majority of apoptotic HCE nuclei. **G:** Morphological features of karyorrhexis were detected only in very few apoptotic HCE-nuclei (≈1%).

tive parameters reveal different response kinetics during the first 2 h of nuclear apoptosis. While S′ and **I/A** reach a saturation level after 10–20 min, Haralicks Entropy, the 2nd Angular Moment, and $\mathbf{P^2/A}$ monitor shape- and structural reorganization up to ≈2 h. Nuclear pyknosis instead is restricted to a time interval between 20–50 min. The obvious difference in the kinetics of the detected phenotypic characteristics suggests that STS induced nuclear

changes enclose a combination of defined molecular events.

During apoptosis, different morphological changes of nuclear structures have been described. For many of them, effector caspases, the mitochondrial apoptosis inducing factor (AIF), or the lysosomal factor cathepsin B have been suggested to play a central role (23,24). The liberation of cathepsin B from lysosomes is reported to involve the release of cytochrome c and caspase-3 from the mitochondria (28). In HCE cells, neither mitochondrial breakdown nor active caspase-3 could be detected prior to the peripheric chromatin condensation. Therefore, effector caspases should be dispensable for early nuclear changes in our system. Instead, a row of observations suggest that AIF could be the responsible initiator of the observed chromatin condensation (23,24,29,30): (i) STS induces AIF translocation from mitochondria into the cytosol and the nucleus, independent of mitochondrial breakdown or the release of caspases or cytochrome c at a first instance; (ii) AIF acts very fast after addition to cell free nuclei and induces only large DNA fragments (>50 kbp); and (iii) AIF initiates PS translocation without the necessity of caspases. None of these findings contradict our data.

Besides the particular chronological order and the selective expression of the apoptotic parameters in HCE cells, Figures 2–4 demonstrate several general benefits of QFM for the study of apoptotic events in adherently growing cell cultures. For the statistical classification of apoptosis, flow cytometry in combination with AV/PI staining has proved to be a reliable method for cell populations, which grow in suspension or provide only weak adhesion forces. Instead, adherently growing cell cultures must be detached actively from their substrate. Harvesting procedures imply stress, which becomes explicitly relevant when disintegrating apoptotic or necrotic cells are concerned (22,25). Cellular disintegration, the detachment of apoptotic bodies from cells, or agent induced vesicle shedding makes it difficult to distinguish by flow cytometry, if AV/PI signals are derived from debris or cells. In a recent publication we have shown that QFM quantifies PS translocation reliably in semi-adherent EL4 cells (21). Here, we present noninvasive QFM as a sensitive method to classify normal, apoptotic, necrotic, and secondary necrotic subpopulations in a cell culture, which strongly attaches to the substrate.

Last but not least, several texture sensitive descriptors clearly separate healthy from apoptotic nuclear structures in HCE cells (see signal to noise ration in Fig. 3B,C). While hyperchromicity has already been reported to be accessible by in situ laser scanning cytometry (22), the use of purely morphologic or texture sensitive descriptors presents an attractive alternative for sensitive, rapid cell screening: (i) textural descriptors are very flexible; the presented parameters are only representatives of a huge family of possible descriptors for different structural organization pattern in selected image regions (16,31); (ii) textural changes can be detected independent of hyperchromicity; they could also be calculated from digital bright field or contrast enhanced microscopy images; (iii) texture sensitive parameters reveal more subtle characteristics than parameters like **A**, **I/A**, or $\mathbf{P^2/A}$ which are easily accessible for any observer; these parameters can help to quantify subtle characteristics and kinetics of phenotypic features which otherwise might not be detected visually.

CONCLUSION

Our study characterizes for the first time apoptotic key features in immortalized HCE cells, which are important for the use of this cell line in biological or toxicology studies. Size-, morphology-, and texture-sensitive parameters detected instant hyperchromicity, peripheric chromatin condensation and nuclear pyknosis upon STS activation. While nuclear changes effected the entire cell population and were completed within 10–120 min, only about 50% of the cells translocated PS in a time interval between ≈2–4 h. Commercially available assays detected significant DNA fragmentation 2 h after STS induction, while caspase-3 activation and decreased mitochondrial viability was detected at 4 h. The rapid quantification of active nuclear reorganization in HCE cells should stimulate further investigation of the observed characteristics in alternative cell systems.

ACKNOWLEDGMENTS

We are indebted to Edda Toma and Christina Kenst for technical assistance. The HCE cell line was a generous gift from Araki-Sasaki and coworkers. S.H. is a Feodor-Lynen-Fellow of the Alexander v. Humboldt Foundation.

LITERATURE CITED

1. Wyllie AH, Kerr JF, Currie AR. Cell death: the significance of apoptosis. Int Rev Cytol 1980;68:251–306.
2. Mirkes PE. To die or not to die, the role of apoptosis in normal and abnormal mammalian development. Teratology 2002;65:228–239.
3. Siao C, Tsirka S. Extracellular proteases and neuronal cell death. Cell Mol Biol 2002;48:151–161.
4. Nickells RW, Zack DJ. Apoptosis in ocular diseases: a molecular overview. Ophthalmic Genet 1996;17:145–165.
5. Gao J, Gelber-Schwalb T, Addeo JV, Stern ME. Apoptosis in the rabbit cornea after photorefractive keratectomy. Cornea 1997;16:200–208.
6. Wilson SE, Pedroza L, Beuerman R, Hill JM. Herpes simplex virus type-l infection of corneal epithelial cells induces apoptosis of the underlying keratocytes. Exp Eye Res 1997;64:775–779.
7. Wickert H, Zaar K, Grauer A, John M, Zimmermann M, Gillardon F. Differential induction of proto-oncogene expression and cell death in ocular tissues following ultraviolet irradiation of the rat eye. Br J Ophthalmol 1999;83:25–230.
8. Mohan RR, Liang Q, Kim WJ, Helena MC, Baerveldt F, Wilson SE. Apoptosis in the cornea: further characterization of Fas/Fas ligand system. Exp Eye Res 1997;65:575–589.
9. Stuart PM, Griffith T, Usui N, Pepose I, Yu X, Ferguson TA. CD95 ligand (FasL)– induced apoptosis is necessary for corneal allograft survival. J Clin Invest 1997;99:396–402.
10. Araki-Sasaki K, Ohashi Y, Sasabe T, Hayashi K, Watanabe H, Tano Y, Handa H. An SV40-immortalized human corneal epithelial cell line and its characterization. Invest Ophthalmol Vis Sci 1995;36:614–621.
11. Meyer T, Regenass U, Fabbro D, Alteri E, Rosel J, Muller M, Caravetti G, Matter A. A derivative of staurosporine (CPG 41 251) shows selectivity for protein kinase C inhibition and in vitro anti-proliferative as well as in vivo anti-tumor activity. Int J Cancer 1989;15:851–856.
12. Ishiyama M, Tominaga H, Shiga M, Sasamoto K, Ohkura Y, Ueno K, Watanabe M. Novel cell proliferation and cytotoxicity assays using a tetrazolium salt that produces a water-soluble formazan dye. In Vitro Toxicol 1995;8:187–189.
13. Kizaki H, Shimada H, Ohsaka F, Sakurada T. Adenosine, deoxyadenosine, and deoxyguanosine induce DNA cleavage in mouse thymocytes. J Immunol 1988;141:1652–1657.
14. Jamitzky F, Stark RW, Bunk W, Thalhammer S, Räth C, Aschenbrenner

T, Morfill GE, Heckl WM. Scaling-index method as an image processing tool in scanning-probe microscopy. Ultramicroscopy 2001;86: 241–246.
15. Castleman KR. Digital image processing. 2nd ed. Englewood Cliffs, NJ: Prentice-Hall; 1996.
16. Haralick RM, Schanmugan K, Dinstein I. Textural features for image classification. IEEE Trans Syst Man Cybernet 1973;SMC-3:610–621.
17. Fadok VA, Voelker DR, Campbell PA, Cohen JJ, Bratton DL, Henson PM. Exposure of phosphatidylserine on the surface of apoptotic lymphocytes triggers specific recognition and removal by macrophages. J Immunol 1992;148:2207–2216.
18. Darzynkiewicz Z, Juan G, Li X, Gorczyca W, Murakami T, Traganos F. Cytometry in cell necrobiology: analysis of apoptosis and accidental cell death (necrosis). Cytometry 1997;27:1–20.
19. Joo C, Cho K, Kim H, Choi JS, Oh YJ. Protective role for bcl-2 in experimentally induced cell death of bovine corneal endothelial cells. Ophthalmic Res 1999;31:287–296.
20. Budd SL, Tenneti L, Lishnak T, Lipton SA. Mitochondrial and extramitochondrial apoptotic signaling pathways in cerebrocortical neurons. Proc Natl Acad Sci USA 2000;97:6161–6166.
21. Jessel R, Haertel S, Socaciu C, Tykhonova S, Diehl HA. Kinetics of apoptotic markers in exogenously induced apoptosis of EL4 cells. J Cell Mol Med 2002;6:82–92.
22. Bedner E, Li X, Gorczyca W, Melamed MR, Darzynkiewicz Z. Analysis of apoptosis by laser scanning cytometry. Cytometry 1999;35:181–195.
23. Susin SA, Lorenzo HK, Zamzami N, Marzo I, Snow BE, Brothers GM, Mangion I, Jacotot E, Costantini P, Loeftler M, Larochette N, Goodlett DR, Aebersold R, Siderovski DP, Penninger IM, Kroemer G. Molecular characterization of mitochondrial apoptosis inducing factor. Nature 1999;397:441–446.
24. Zamzami N, Kroemer G. Condensed matter in cell death. Nature 1999;401:127–128.
25. Van Engeland M, Nieland LJ, Ramaekers FC, Schutte B, Reutelingsperger CP. Annexin-V–affinity assay: a review on an apoptotic detection system based on PS exposure. Cytometry 1998;1:1–9.
26. Zwaal RFA, Schroit AJ. Pathophysiologic implications of membrane phospholipid asymmetry in blood cells. Blood 1997;89:1121–1132.
27. Poot M, Gibson L, Singer V. Detection of apoptosis in live cells by MitoTracker Red CMXRos and SYTO dye flow cytometry. Cytometry 1997;27:358–364.
28. Kessel D, Luo Y, Mathieu P, Reiners JJ. Determinants of the apoptotic response to lysosomal photodamage. Photochem Photobiol 2000;71: 196–200.
29. Cande C, Cohen I, Daugas E, Ravagnan L, Larochette N, Zamzami N, Kroemer G. Apoptosis-inducing factor (AIF): a novel caspase-independent death effector released from mitochondria. Biochimie 2002;84: 215–22.
30. Daugas E, Nochy D, Ravagnan L, Loeffler M, Susin SA, Zamzami N, Kroemer G. Apoptosis-inducing factor (AIF): a ubiquitous mitochondrial oxidoreductase involved in apoptosis. FEBS Lett 2000;476:118–23.
31. Lehmann T, Oberschelp W, Pelikan E, Repges R. Bildverarbeitung für die Medizin. Heidelberg: Springer-Verlag; 1997.